Evaluation of the nominal thickness of pipelines using neural networks through the dispersion curves drawn with the SAFE method

Daniel Boechat, Barbara V. A. Lavor, Paula A. Sesini, Helon V. H. Ayala, Arthur M. B. Braga
Department of Mechanical Engineering
Pontificia Universidade Católica do Rio de Janeiro
Rio de Janeiro, Brazil
dboechat.m@gmail.com

***Abstract*—Inspection through non-destructive testing is important for the analysis of oil well structures in different phases of the project, whether during execution, during the production period, or at closure. In this context, the propagation of ultrasonic waves is an important ally to assessing the integrity of structural components, through the tracing of dispersion curves, which show the pair frequency x wavelength for a specific waveguide. This study presents a neural network framework for estimating the percentage of nominal pipeline thickness. The neural network inputs are dispersion curves obtained by simulation, using the semi-analytical finite element method (SAFE), that presents a computational cost reduced compared with the totally numerical simulation. In this way, 100 samples were generated. The case studied consists of a hollow cylinder with different thickness sizes. From the results, it is concluded that the adopted methodology is efficient to predict the percentage of nominal pipeline thickness.**

***Index Terms*—Non-destructive testing, pipelines, SAFE, Machine Learning, Neural Networks.**

I. Introduction

Petroleum derivatives represent a large portion of the world's energy matrix. Their exploitation, transport, plugging, and abandonment operations at the end of the well's production cycle require dedication to risk management and ensuring the safety of activities [1], [2].

Offshore pipelines are large structures costing hundreds of millions of dollars [3]. Taking into account factors such as the location where the line is installed, the significant value of the transported commodity, and its composition, it is easy to imagine the consequence of a failure that leads a structure to ruin which, in addition to having catastrophic environmental impacts, can also represent financial losses and even lead to the loss of human lives. It is important to prevent those accidents and, above all, to guarantee the physical integrity of people. So, the responsibility of the team involved in the project is great. Therefore, these projects demand and deserve the care and attention that modern engineering tools can provide.

There are several types of damage that can affect these structures, such as localized collapse due to buckling, caused by factory ovality aggravated during installation/operation [4], external pressure and internal pressure variations, the generation of a dent due to impacts with objects (such as the anchor or a piece of equipment dropped from a vessel operating in the area, for example) and detrition due to corrosion or erosion [5], [6].

In this sense, carrying out maintenance and inspections is part of the routine of the oil and gas industry [7]–[9]. Therefore, non-destructive techniques such as ultrasound inspections are used. Also, their development and improvement is still an object of study and technological advances, as they allow testing with the least amount of interference.

The propagation of ultrasonic waves is an important tool to measure the integrity of structures [10]–[12]. In non-destructive tests, acoustic pulses that propagate through the structure are emitted. By comparing the behavior of mechanical waves, as to how they propagate in a healthy environment, and the characteristics of the medium read from the signal registered in the receivers, it is possible to identify damage in the coating layers, since the occurrence of defects influences the shape of the dispersion curves and the guided modes.

However, solving the systems of equations needed to trace the dispersion curves requires a certain computational cost.

In recent years, semi-analytical methods have been used. With these methods, an analytical solution is used in the longitudinal coordinate, while a numerical one is still adopted for the behavior in the cross-section plane. In this way, the numerical effort is reduced, and so the computational cost, compared to fully numerical methods.

An example is presented in [13] where the computation time reduction of the simulation and analysis of waveguide dispersion curves are studied. The proposed method, which consists of building sets of Kriging metamodels using WFEM (Wave/Finite Element Method) representations, shows promising results. In [14] a semi-analytical finite element (SAFE) method for the simulation of wave propagation in waveguides of an arbitrary cross-section is investigated. The proposed SAFE formulation is applied to different cases: anisotropic viscoelastic layered boards, composite-to-composite adhesive joints, and railroad tracks. In [15], how conventional finite element modal analysis of a layer of an infinite homogeneous or periodic waveguide supplies fundamental information on its properties is demonstrated. A novel method is proposed to

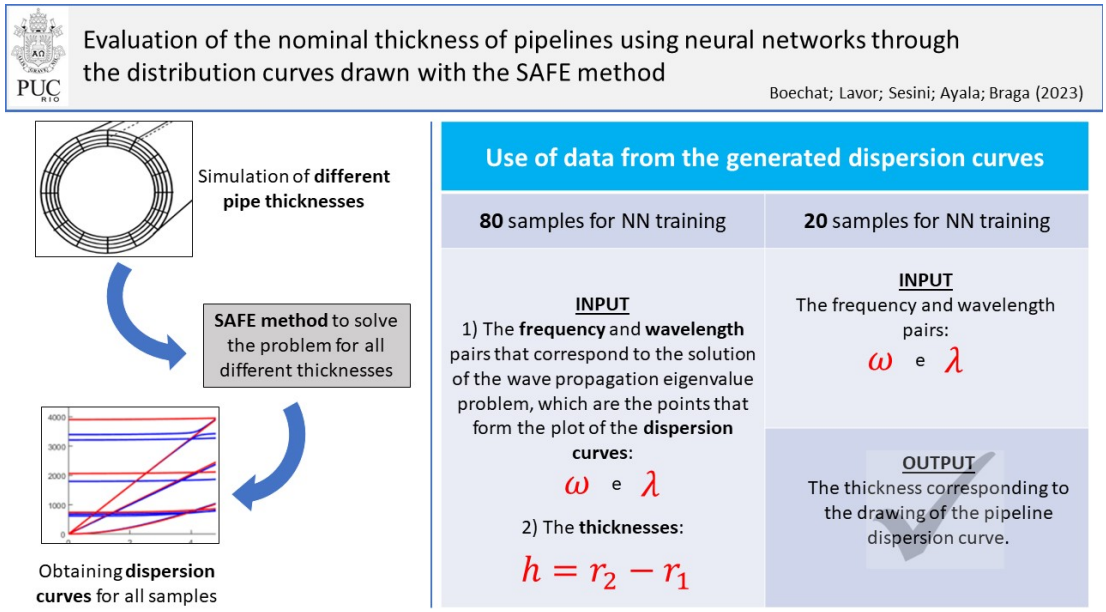

Fig. 1. This Graphical Abstract presents in a synthetic way how this study was carried out to evaluate the nominal thickness of pipelines using neural networks trained with dispersion curves obtained by the SAFE method.

evaluate the decay rates caused by material losses.

Although the aforementioned works propose effective solutions for the simulation of wave propagation in pipelines, the computational cost is an aspect that requires more investigation. In this context, here it is proposed to use the semi-analytical finite element method (SAFE) for the simulation of wave propagation in waveguides with cylindrical structures. A harmonic analytical solution in the axial and angular directions is used, and the finite element method is in the radial direction. In this way, the resulting problem is unidimensional, which represents a reduction in the computational cost compared with the bidimensional approaches. In the implementation published by [16] of the SAFE method, there was an interesting reduction in the computational cost for obtaining the dispersion curves of a cylinder: using a commercial finite element software, the processing time was over 1 day and 5 hours, while the semi- analysis took only 8 minutes.

The SAFE method mentioned above was implemented in Matlab and due to the low computational cost inherent to this method, this same implementation was used to generate simulations whose data served as input for the machine learning. The progress in machine learning techniques allows the reduction of human intervention in the analysis of detected defects [17]–[20]. Among the various techniques that have been developed a Convolutional Neural Network (CNN) technique is a genre of neural networks that have already demonstrated excellent capabilities in tasks such as pattern recognition, computer vision [21], and time series classification [22], proving its ability to deal with complex and nonlinear problems [23], [24]. It is designed to automatically learn and extract features from images, allowing it to perform tasks such as object recognition, segmentation, and classification [25]–[27].

Combining the use of a semi-analytical method to obtain input data with machine learning to evaluate samples can bring more agility to the analysis of results and reduce the need to provide resources for data collection and assembly of experimental test rigs [17]. Obviously, it is not suggested to dispense with these alternatives but to complement and improve them.

This study aims to develop a deep learning-based framework for estimating the nominal thickness of pipelines by utilizing the dispersion curves obtained through the SAFE method. The motivation behind this research is to save time and reduce financial costs. To accomplish this, a series of numerical simulation experiments were performed, resulting in 100 different responses of dispersion curves associated with each nominal thickness of pipelines. A CNN architecture is proposed, and its performance is evaluated using various regression metrics.

The organization of this work follows the sequence: In this Section I, the subject was presented in general terms, and a graphical abstract is shown in Fig 1, in Section II the description of the case study is presented, in Section III the methods employed are explained, in Section IV describes the achieved results, and finally, Section V presents the final considerations.

II. Problem Analyzed

The structure analyzed is a stress-free hollow cylinder like the one shown in Fig 2 with linear elastic material behavior and an initial thickness of 0.03 m. As 100 simulations were used, each one had a variation of 2.0×10^{-5} m in the initially adopted thickness. For each of these cylinders, there is an associated set of dispersion curves. These scatter curves were used as input for machine learning training. The

SAFE method was implemented in Matlab [16], using one-dimensional elements in the radial direction of the cylinder's cross-section and the analytical solution in the longitudinal and circumferential directions. The dispersion curves obtained by [16], are shown in Fig. 3, where the ratio h/λ is the frequency by dimensionless wavelength, h is the thickness of the cylinder and λ is the wavelength.

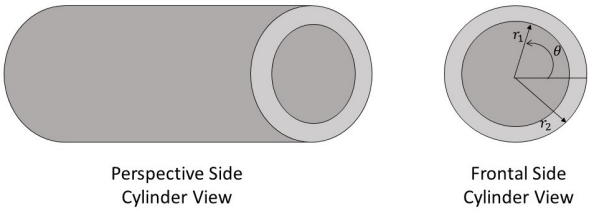

Fig. 2. The stress-free hollow cylinder model used.

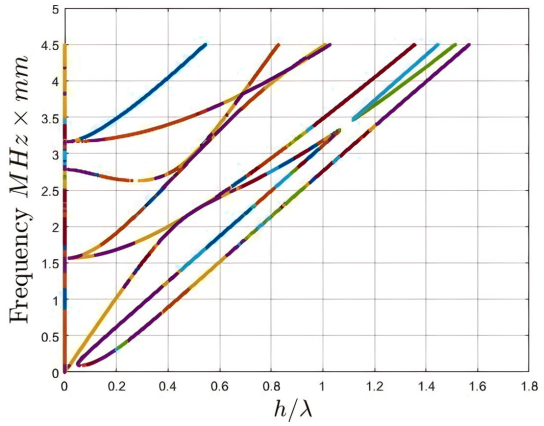

Fig. 3. The dispersion curves for a hollow cylinder was calculated using the SAFE method.

III. Methodology

A. Semi-Analytical Finite Element Method (SAFE)

In very long waveguides, such as railtrain tracks, or oil wells production pipelines, the study of elastic wave propagation can result in high computational costs due to the discretization necessary to represent the wavelengths in the longitudinal direction [3], [28], [29]. Using the SAFE method, as already stated in this work, the discretization of the structure in finite elements is done in the radial direction, obtaining an approximate displacement field. Along both the circumferential and the longitudinal direction, the analytical solution with the harmonic representation of the wave in the time domain is used [16].

Using the semi-analytical approach, the displacement field that represents the wave motion is considered as follows:

$$\boldsymbol{u}^{(e)}(r,\theta,z,t) = \sum_{j=1}^{n} \mathbf{N}(r)\mathbf{q}^{(e)} e^{i(kz+n\theta-\omega t)}, \tag{1}$$

where $\mathbf{u}^{(e)}$ is the displacement field, r, θ e z are the cylindrical coordinates, $\mathbf{q}^{(e)}$ is the nodal displacement vector, k is the wave number in the axial direction, n is an integer in the circumferential harmonic, ω is the frequency, and t corresponds to time. The shape functions $\mathbf{N}$ that corresponds to the finite element, is given by:

$$\mathbf{N} = \begin{bmatrix} N_1 & 0 & 0 & N_2 & 0 & 0 \\ 0 & N_1 & 0 & 0 & N_2 & 0 \\ 0 & 0 & N_1 & 0 & 0 & N_2 \end{bmatrix}, \tag{2}$$

with linear shape function

$$N_1 = \frac{1}{2}(1-\xi) \quad \text{and} \quad N_2 = \frac{1}{2}(1-\xi). \tag{3}$$

The eigenvalue problem in the global coordinate system is represented in the following equation:

$$\left(\mathbf{K}_1 + ik\mathbf{K}_2 + k^2\mathbf{K}_3 - \omega^2\mathbf{M}\right)\mathbf{Q} = 0, \tag{4}$$

with

$$\begin{aligned} \mathbf{K}_1^{(e)} &= \int_r \int_\theta \mathbf{B}_1^T \mathbf{C}\mathbf{B}_1 \, r \, dr \, d\theta \\ \mathbf{K}_2^{(e)} &= \int_r \int_\theta \left(\mathbf{B}_1^T \mathbf{C}\mathbf{B}_2 - \mathbf{B}_2^T \mathbf{C}\mathbf{B}_1\right) r \, dr \, d\theta \\ \mathbf{K}_3^{(e)} &= \int_r \int_\theta \mathbf{B}_2^T \mathbf{C}\mathbf{B}_2 \, r \, dr \, d\theta \\ \mathbf{M}^{(e)} &= \rho \int_r \int_\theta \mathbf{N}^T \mathbf{N} \, r \, dr \, d\theta \end{aligned} \tag{5}$$

where $\mathbf{K}_1$, $\mathbf{K}_2$ and $\mathbf{K}_3$ are the equivalent stiffness matrices; matrix $\mathbf{B}$ represents the geometric compatibility matrix, composed of the shape functions and their derivatives; matrix $\mathbf{C}$ is the constitutive tensor for elastic materials; $\mathbf{M}$ is the global mass matrix; $\mathbf{Q}$ is the global displacement vector; k is the wave number in the axial direction and ω is the frequency.

B. Convolutional Neural Network (CNN)

The CNN is an advanced Artificial Neural Network (ANN) defined as a representative deep learning framework based on a visual perception engine and convolutional computation [30]. Being different from traditional ANN, CNN can directly capture the spatial features from images to improve both prediction accuracy and efficiency [31]. The CNN has been widely employed in diverse fields such as computer vision including image classification [32], object tracking, visual salience detection, action recognition; natural language processing [33] and time series classification and forecasting [22], [30], [34].

The main CNN structure includes a convolutional layer, pooling layer, and fully connected layer.

In the convolutional layer, a neuron is connected to only a portion of the neighboring neurons, which reduces the complexity of the network and the number of parameters [30]. This layer is used to extract the features of input images by applying a set of filters to the input data, producing a set of output feature maps [34]. As observed in Equation 6,

which represents the convolutional layer equation and filters are applied to the input matrix.

$$\mathbf{y}_{ij}^{(l)} = \mathbf{f}\left(\sum_{m=1}^{M}\sum_{n=1}^{N}\mathbf{W}_{mn}^{(l)} \cdot \mathbf{x}_{(i+m)(j+n)}^{(l-1)} + \mathbf{b}^{(l)}\right) \quad (6)$$

where, $\mathbf{x}$ denotes the input matrix, capturing the input data. The learnable weights $\mathbf{W}$ are convolutional filters applied to the input matrix, with the specific filter sizes and the number of filters depending on the problem at hand. The bias term $\mathbf{b}$ is added to the convolutional operation. The resulting output $\mathbf{y}$ is obtained by applying the activation function $\mathbf{f}$ element-wise to the output of the convolutional operation and the index l represents the layer in the convolutional neural network on which the operation is being performed.

The pooling layer is employed to reduce the dimensions of the feature maps to maintain relevant information of the cross-sectional frame images obtained from the convolutional layer [35]. In this regression problem, the pooling layer can be applied after the convolutional layer. The input to the pooling layer can be the output from the convolutional layer, resulting in a reduced size representation increasing the computation speed. This operation helps to avoid over-fitting [30]. The type of pooling used and the size of the pooling window can affect the network's ability to detect specific features.

There are mainly two types of pooling: maximum pooling and average pooling. Maximum pooling selects the maximum values from a specified kernel applied to the image, while average pooling computes the average value within the kernel specified over the image [36]. These pooling methods play a crucial role in downsampling the feature maps, enabling the extraction of dominant features while reducing the spatial dimensions [37].

The fully connected layer classifies the extracted features from the previous layers [22]. It focuses on the transformation of the pooled features into a suitable representation for regression. The pooled features are flattened into a one-dimensional vector and then connected to a fully connected layer [36]. It introduces the matrix multiplication between the fully connected layers, as represented in Equation 7, and the activation function (σ) applied to this output. This layer finalizes the transformation of the extracted features into a final prediction.

$$\mathbf{y}^{(l)} = \sigma\left(\mathbf{W}^{(l)} \cdot \mathbf{x}^{(l-1)} + b^{(l)}\right) \quad (7)$$

In this architecture, the number of neurons in the fully connected layers can be customized based on the complexity of the regression problem. The activation functions in the fully connected layers can be chosen based on the problem requirements, such as ReLU or tanh, enabling non-linear mappings between the features and the target values.

C. Proposed CNN architecture

In this work, we proposed a CNN architecture based on LeNet-5 to estimate the pipeline thickness. The architecture of the CNN consisted of two convolutional layers, two max pooling layers, two fully connected layers, and one output layer, as depicted in Fig. 4. For this model, we used a 2D array as input data. Therefore, as the simulation result in a 2048x66 data pre-processing has to be done by feature selection based on variance to reduce the amount of data. As a result, a 2048x32 matrix was obtained and used as input data. Each simulation was considered as a sample for the model training and validation. In the CNN, another automatic feature extraction was performed by two sets of convolutional layers followed by max pooling layers.

To define the ideal structure of the CNN, a grid search was performed varying the filters in the convolutional layers, the kernel size, and the max pooling size. For the dense layers, sizes 120 and 84 nodes were used. Only the ReLu function was used as an activation function in the dense layer.

IV. Results and Discussion

This section focuses on the evaluation of the performance of the proposed CNN architecture. To assess its effectiveness, several regression metrics were employed, including the Root Mean Squared Error (RMSE), Mean Absolute Error (MAE), and Maximum Error (MAXE). The equations for these metrics are presented below:

Root Mean Squared Error (RMSE):

$$\text{MAE} = \frac{1}{n}\sum_{i=1}^{n}|y_i - \hat{y}_i| \quad (8)$$

Mean Absolute Error (MAE):

$$\text{RMSE} = \sqrt{\frac{1}{n}\sum_{i=1}^{n}(y_i - \hat{y}_i)^2} \quad (9)$$

Maximum Error (MAXE):

$$\text{MAXE} = \max_i |y_i - \hat{y}_i| \quad (10)$$

where $\mathbf{y_i}$ represents the true values, $\hat{\mathbf{y}}_\mathbf{i}$ represents the predicted values, and $\mathbf{n}$ represents the number of samples.

A. Hyperparameter selection

A grid search method was used as the hyperparameter selection process. The datasets were randomly divided into a training dataset containing 80% of the samples and a test dataset containing the remaining 20%.

Table I summarizes the results obtained throughout the test phase. Both the RMSE and MAE are metrics that measure the average magnitude of the error between the actual and predicted values. The difference is that the RMSE is a quadratic rule that gives high weight to higher errors and MAE gives a measure of the average magnitude of the error, ignoring the direction of the errors.

The results show that the mean RMSE was higher than the mean MAE indicating variations in the magnitude of the errors. Despite that, both metrics were close to the ideal value of 0.0. The MAXE represents the maximum error for a set of

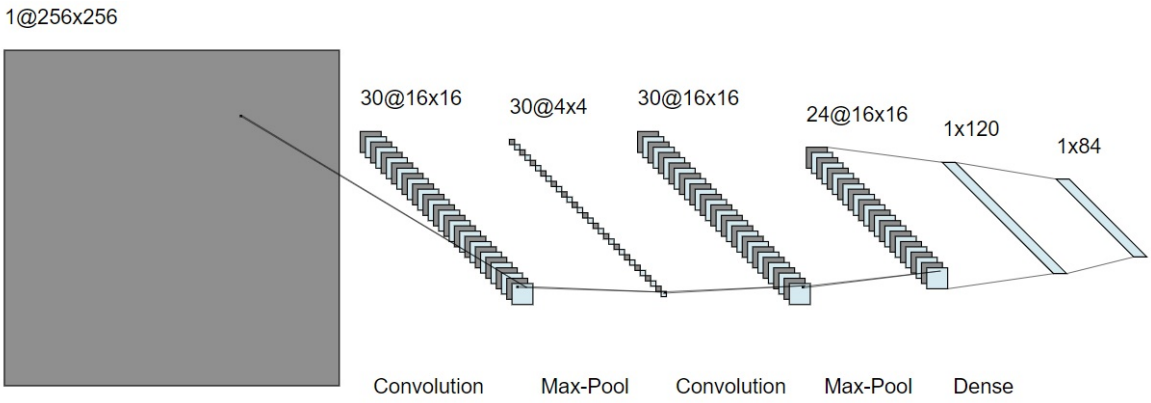

Fig. 4. Schematic representation illustrating the preprocessing procedure and the architecture of the proposed CNN for evaluating the nominal thickness of pipelines.

TABLE I
REGRESSION METRICS OBTAINED OF PREDICTED PIPELINES THICKNESS

Conv. Filter	Kernel Size	Max Pool Size	**RMSE**	**MAE**	**MAXE**
5	8	2	0.015423	0.000238	0.01728
5	8	4	0.016153	0.000261	0.018012
5	16	2	0.014697	0.000216	0.016551
5	16	4	0.006617	0.000044	0.010102
5	32	2	0.015045	0.000226	0.0169
5	32	4	0.012906	0.000167	0.014754
15	8	2	0.017342	0.000301	0.019204
15	8	4	0.011582	0.000134	0.016487
15	16	2	0.011185	0.000125	0.013116
15	16	4	0.010304	0.000106	0.012862
15	32	2	0.014977	0.000224	0.016832
15	32	4	0.013527	0.000183	0.015378
30	8	2	0.015541	0.000242	0.017398
30	8	4	0.012125	0.000147	0.013272
30	16	2	0.014913	0.000222	0.016769
30	**16**	**4**	**0.002401**	**0.000006**	**0.007419**
30	32	2	0.011271	0.000127	0.013111
30	32	4	0.01225	0.00015	0.014096

test samples. The fact that the mean MAXE value was higher than 1.0 indicates that some of the models committed relatively large errors.

Analyzing Fig. 5 and Fig. 6, it can be seen that the model converges quickly in a few iterations. A sign of over-fitting such as loss of validation was not observed, due to the non-occurrence of the increase in error prediction. This is important information to evaluate the quality of the model and can be used to justify the choice of a specific training approach or model configuration.

Fig. 7 and 8 show that despite having used small data set for training, the model is able to make reasonably good predictions in the testing phase. As seen in the figure, the model provided an good approximation between the predicted and actual values. The result of the model with the best performance is presented in table I. For this case, the RMSE, MAE, and MAXE were equal to 0.002401, 0.000006, and 0.007419, respectively.

V. FINAL CONSIDERATIONS

In this work, the SAFE method implemented in MATLAB was used to generate dispersion curves referring to cylindrical waveguides with different thicknesses. The pair of frequencies and wave numbers, referring to the curves obtained, served as input data for machine learning with the technique of convolutional neural networks.

The results referring to the training indicate that the model converges faster, that is, with few iterations. Furthermore, there are no signs of overfitting as the validation metric does not get worse, indicating a good generalization for studies of cylindrical waveguides with different thicknesses.

Although little data was used, the prediction graph shows that the model is able to predict reasonably well in the test phase for an out-of-envelope data condition used in training. The RMSE is suitable for practical applications and the prediction in the training phase indicates that it is still possible to improve this value.

With what was observed and reported in this work, it can be highlighted that the use of the results of the SAFE method has the potential to save time and reduce financial costs and exposure to risk for workers, since the use of studies with numerical and computational simulation provided obtaining a sufficient number of data. This would avoid the mandatory installation of experimental test rigs or the displacement of teams to collect data *in situ*.

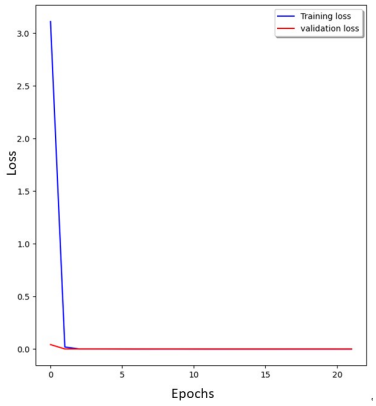

Fig. 5. Training and test LOSS over epochs.

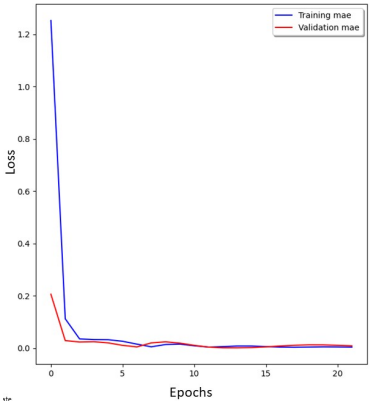

Fig. 6. Training and test MAE over epochs.

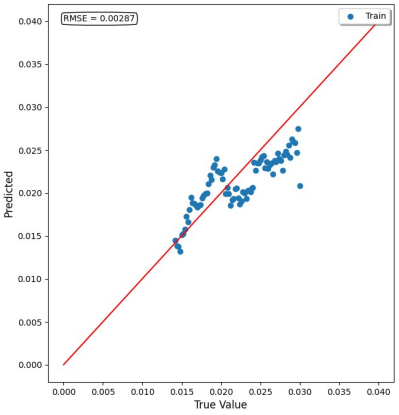

Fig. 7. Train predictions Scatter

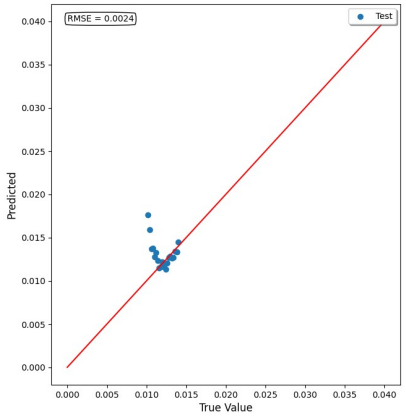

Fig. 8. Test predictions Scatter

ACKNOWLEDGMENT

The authors would like to express their gratitude for the financial support provided by CNPq (National Council for Scientific, Technological Development) and CAPES (Coordination of Superior Level Staff Improvement) and the Brazilian National Agency for Petroleum, Natural Gas and Biofuels (ANP) through the Human Resources Program for the Petroleum, Natural Gas and Biofuels sector - PRH-ANP.

REFERENCES

[1] C. Chen, C. Li, G. Reniers, F. Yang, Safety and security of oil and gas pipeline transportation: A systematic analysis of research trends and future needs using wos, Journal of Cleaner Production 279 (2021) 123583.

[2] Y. Su, J. Li, B. Yu, Y. Zhao, J. Yao, Fast and accurate prediction of failure pressure of oil and gas defective pipelines using the deep learning model, Reliability Engineering & System Safety 216 (2021) 108016.

[3] S. Kyriakides, E. Corona, Mechanics of offshore pipelines: volume 1 buckling and collapse, Vol. 1, Elsevier, 2007.

[4] J. L. d. F. Freire, Engenharia de dutos, ABCM–Associação Brasileira de Engenharia e Ciências Mecânicas. Rio de Janeiro (2009) 15–1.

[5] D. J. S. Cunha, C. Ferraz, T. A. Netto, D. G. G. Rosa, J. L. F. Freire, Hydrostatic collapse tests of full-scale pipeline specimens with thickness metal loss, International Pipeline Conference - IPC2020 2 (13) (2020).

[6] D. G. G. Rosa, D. J. S. Cunha, J. C. Diniz, C. Ferraz, T. A. Netto, R. D. Vieira, J. L. d. F. Freire, Previsão de pressão de colapso em dutos sob pressão externa, Conferencia Internacional sobre Evaluación de Integridad y Extensión de Vida de Equipos Industriales - CONAENDI-IEV 1 (22) (2020).

[7] J. Xin, R. Li, J. Chen, R.-k. Lu, C. Liu, Z. Su, R. He, H. Zhu, A crack characterization model for subsea pipeline based on spatial magnetic signals features, Ocean Engineering 274 (2023) 114112.

[8] Y. Zhang, T. Tan, Z. Xiao, W. Zhang, M. Ariffin, Failure assessment on offshore girth welded pipelines due to corrosion defects, Fatigue & Fracture of Engineering Materials & Structures 39 (4) (2016) 453–466.

[9] B.-Q. Chen, X. Zhang, C. G. Soares, The effect of general and localized corrosions on the collapse pressure of subsea pipelines, Ocean Engineering 247 (2022) 110719.

[10] W. M. Alobaidi, E. A. Alkuam, H. M. Al-Rizzo, E. Sandgren, et al., Applications of ultrasonic techniques in oil and gas pipeline industries: A review, American Journal of Operations Research 5 (04) (2015) 274.

[11] A. Carvalho, J. Rebello, M. Souza, L. Sagrilo, S. Soares, Reliability of non-destructive test techniques in the inspection of pipelines used in the oil industry, International journal of pressure vessels and piping 85 (11) (2008) 745–751.

[12] E. Pan, J. Rogers, S. Datta, A. Shah, Mode selection of guided waves for ultrasonic inspection of gas pipelines with thick coating, Mechanics of Materials 31 (3) (1999) 165–174.

[13] B. Zhu, L. Nechak, O. Bareille, Kriging metamodeling approach for predicting the dispersion curves for wave propagating in complex waveguide, Journal of Sound and Vibration (2023) 117595.

[14] I. Bartoli, A. Marzani, F. L. Di Scalea, E. Viola, Modeling wave propagation in damped waveguides of arbitrary cross-section, Journal of sound and vibration 295 (3-5) (2006) 685–707.

[15] S. Sorokin, P. Broberg, M. Steffensen, L. Ledet, Finite element modal analysis of wave propagation in homogeneous and periodic waveguides, International Journal of Mechanical Sciences 227 (2022) 107444.

[16] B. Lavor, P. Sesini, A. Braga, A comparative study of dispersion curves in cylindrical waveguide using the semi-analytical finite element method, DINAME 2023. Pirinopolis (2023).

[17] Y. Liu, Y. Bao, Review on automated condition assessment of pipelines with machine learning, Advanced Engineering Informatics 53 (2022) 101687.
[18] A. H. Alamri, Application of machine learning to stress corrosion cracking risk assessment, Egyptian Journal of Petroleum 31 (4) (2022) 11–21.
[19] A. A. Soomro, A. A. Mokhtar, J. C. Kurnia, N. Lashari, H. Lu, C. Sambo, Integrity assessment of corroded oil and gas pipelines using machine learning: A systematic review, Engineering Failure Analysis 131 (2022) 105810.
[20] A. Rachman, T. Zhang, R. C. Ratnayake, Applications of machine learning in pipeline integrity management: A state-of-the-art review, International journal of pressure vessels and piping 193 (2021) 104471.
[21] J. Siavashi, A. Najafi, M. Ebadi, M. Sharifi, A cnn-based approach for upscaling multiphase flow in digital sandstones, Fuel 308 (2022) 122047.
[22] G. Rezende Bessa Ferreira, P. Aida Sesini, L. Paulo Brasil de Souza, A. Conci Kubrusly, H. Vicente Hultmann Ayala, Corrosion-like defect severity estimation in pipelines using convolutional neural networks, in: 2021 IEEE Symposium Series on Computational Intelligence (SSCI), 2021, pp. 01–07.
[23] C. Spandonidis, P. Theodoropoulos, F. Giannopoulos, N. Galiatsatos, A. Petsa, Evaluation of deep learning approaches for oil & gas pipeline leak detection using wireless sensor networks, Engineering Applications of Artificial Intelligence 113 (2022) 104890.
[24] B. Wang, Y. Guo, D. Wang, Y. Zhang, R. He, J. Chen, Prediction model of natural gas pipeline crack evolution based on optimized dcnn-lstm, Mechanical Systems and Signal Processing 181 (2022) 109557.
[25] L. Chen, X. Yao, C. Tan, W. He, J. Su, F. Weng, Y. Chew, N. P. H. Ng, S. K. Moon, In-situ crack and keyhole pore detection in laser directed energy deposition through acoustic signal and deep learning, Additive Manufacturing 69 (2023) 103547.
[26] G. De Masi, R. Vichi, M. Gentile, R. Bruschi, G. Gabetta, A neural network predictive model of pipeline internal corrosion profile, in: Proceedings of the 1st International Conference on Systems Informatics, Modeling and Simulation, 2014, pp. 18–23.
[27] A. Krizhevsky, I. Sutskever, G. E. Hinton, Imagenet classification with deep convolutional neural networks, Communications of the ACM 60 (6) (2017) 84–90.
[28] J. L. Rose, Ultrasonic waves in solid media (2000).
[29] T. Hayashi, W.-J. Song, J. L. Rose, Guided wave dispersion curves for a bar with an arbitrary cross-section, a rod and rail example, Ultrasonics 41 (3) (2003) 175–183.
[30] W. Zha, Y. Liu, Y. Wan, R. Luo, D. Li, S. Yang, Y. Xu, Forecasting monthly gas field production based on the cnn-lstm model, Energy 260 (2022) 124889.
[31] C. Zhu, J. Wang, S. Sang, W. Liang, A multiscale neural network model for the prediction on the equivalent permeability of discrete fracture network, Journal of Petroleum Science and Engineering 220 (2023) 111186.
[32] F. Liu, X. Wang, Z. Liu, F. Tian, Y. Zhao, G. Pan, C. Peng, T. Liu, L. Zhao, K. Zhang, S. Zhang, X. Liu, R. Zhao, Identification of tight sandstone reservoir lithofacies based on cnn image recognition technology: A case study of fuyu reservoir of sanzhao sag in songliao basin, Geoenergy Science and Engineering 222 (2023) 211459.
[33] J. Gu, Z. Wang, J. Kuen, L. Ma, A. Shahroudy, B. Shuai, T. Liu, X. Wang, G. Wang, J. Cai, T. Chen, Recent advances in convolutional neural networks, Pattern Recognition 77 (2018) 354–377.
[34] S. Kwon, G. Park, Y. Jang, J. Cho, M. gon Chu, B. Min, Determination of oil well placement using convolutional neural network coupled with robust optimization under geological uncertainty, Journal of Petroleum Science and Engineering 201 (2021) 108118.
[35] E. T. Brantson, M. Abdulkadir, P. H. Akwensi, H. Osei, T. F. Appiah, K. R. Assie, S. Samuel, Gas-liquid vertical pipe flow patterns convolutional neural network classification using experimental advanced wire mesh sensor images, Journal of Natural Gas Science and Engineering 99 (2022) 104406.
[36] D. S. Rajput, G. Meena, M. Acharya, K. K. Mohbey, Fault prediction using fuzzy convolution neural network on iot environment with heterogeneous sensing data fusion, Measurement: Sensors 26 (2023) 100701.
[37] E. Paul, S. R.S., Modified convolutional neural network with pseudo-cnn for removing nonlinear noise in digital images, Displays 74 (2022) 102258.
[38] A. LeNail, Nn-svg: Publication-ready neural network architecture schematics., J. Open Source Softw. 4 (33) (2019) 747.